Hindawi Publishing Corporation
Journal of Nanomaterials
Volume 2014, Article ID 934165, 7 pages
http://dx.doi.org/10.1155/2014/934165

Research Article

Hydrothermal Synthesis, Characterization, and Optical Properties of Ce Doped Bi_2MoO_6 Nanoplates

Anukorn Phuruangrat,[1] Nuengruethai Ekthammathat,[2] Budsabong Kuntalue,[3] Phattranit Dumrongrojthanath,[2] Somchai Thongtem,[4,5] and Titipun Thongtem[2]

[1] *Department of Materials Science and Technology, Faculty of Science, Prince of Songkla University, Hat Yai, Songkhla 90112, Thailand*
[2] *Department of Chemistry, Faculty of Science, Chiang Mai University, Chiang Mai 50200, Thailand*
[3] *Electron Microscopy Research and Service Center, Faculty of Science, Chiang Mai University, Chiang Mai 50200, Thailand*
[4] *Department of Physics and Materials Science, Faculty of Science, Chiang Mai University, Chiang Mai 50200, Thailand*
[5] *Materials Science Research Center, Faculty of Science, Chiang Mai University, Chiang Mai 50200, Thailand*

Correspondence should be addressed to Anukorn Phuruangrat; phuruangrat@hotmail.com and Titipun Thongtem; ttpthongtem@yahoo.com

Received 14 December 2013; Accepted 17 March 2014; Published 15 April 2014

Academic Editor: Ajay Soni

Undoped and Ce doped Bi_2MoO_6 samples were synthesized by hydrothermal reaction at 180°C for 20 h. Phase, morphology, atomic vibration, and optical properties were characterized by X-ray powder diffraction (XRD), X-ray photoelectron spectroscopy (XPS), Raman spectrophotometry, Fourier transform infrared (FTIR) spectroscopy, scanning electron microscopy (SEM), transmission electron microscopy (TEM), selected area electron diffraction (SAED), and UV-visible spectroscopy. In this research, the products were orthorhombic Bi_2MoO_6 nanoplates with the growth direction along the [0b0], including the asymmetric and symmetric stretching and bending modes of Bi–O and Mo–O. Undoped and Ce doped Bi_2MoO_6 samples show a strong absorption in the UV region.

1. Introduction

Aurivillius family of structurally related oxides with chemical formula of $Bi_2A_{n-1}B_nO_{3n+3}$ (A = Ca, Sr, Ba, Pb, Bi, Na, K, and B = Ti, Nb, Ta, Mo, W, and Fe) was originally attractive material due to its layered structure and unique properties [1, 2]. The perovskite-type blocks lead to variable layers along the *c*-axis due to the integer *n* with $n = 0, 1, 2, 3, 4, 5$ and a typical "mica-like" two-dimensional structure [1]. Bi_2MoO_6 with narrow band gap of 2.9 eV is a typical Aurivillius phase with its structure consisting of perovskite layers $(A_{n-1}B_nO_{3n+1})^{2-}$ between $(Bi_2O_2)^{2+}$ bismuth oxide layers, with a general formula $[Bi_2O_2]$ $[A_{n-1}B_nO_{3n+1}]$ [3, 4]. Bi_2MoO_6 is an interesting material due to its unique physical properties for solar energy conversion, ion conduction, and photocatalysis for water splitting under visible-light irradiation and gas sensors [1, 2]. Various synthetic methods for this material have been reported such as hydrothermal/solvothermal [1, 3, 5], aerosol-spraying [4], coprecipitation [6], thermal evaporation [7], and hard-template method [8]. Recently, rare earth dopants have been excessively applied to modify optical properties of nanomaterials due to their possible transition of 4f electron configuration. Among them, cerium is one of the most interesting dopants due to its different electronic structure between Ce^{3+} ($4f^15d^0$) and Ce^{4+} ($4f^05d^0$), leading to different optical properties. It generates oxygen vacancies and bulk oxygen species, which have relatively high mobility. Thus they are more active for oxidation processes [9, 10].

In this paper, 0–3% Ce doped Bi_2MoO_6 crystallites were successfully synthesized by the hydrothermal process. Phase,

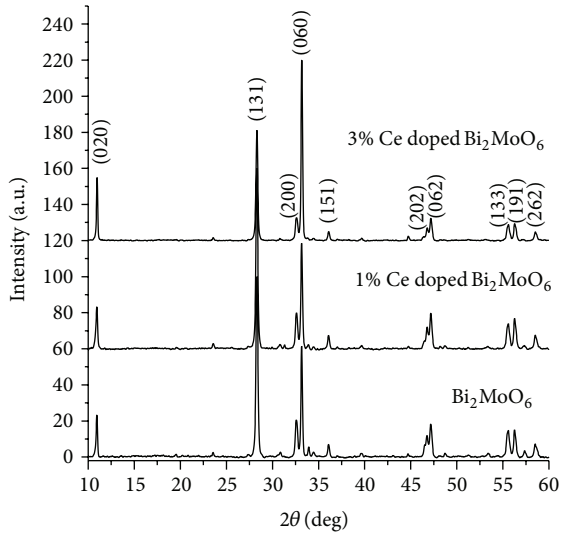

Figure 1: XRD patterns of the undoped, 1% Ce doped. and 3% Ce doped Bi_2MoO_6 samples synthesized by hydrothermal reaction at 180°C for 20 h.

morphologies, and optical properties of the undoped and Ce doped Bi_2MoO_6 crystallites were intensively investigated.

2. Experimental Procedures

All the reagents were of analytical grade and used as received without further purification. In a typical experiment, 0.5 mmol $Na_2MoO_4{\cdot}2H_2O$ and 1 mmol $Bi(NO_3)_3{\cdot}5H_2O$ were dissolved in 60 mL deionized water to form solution A under 20 min magnetic stirring at room temperature. Concurrently, 1 and 3% by weight $Ce(NO_3)_3{\cdot}6H_2O$ were dissolved in 40 mL deionized water each to form solution B under 20 min magnetic stirring at room temperature. Then, solution B was slowly added to solution A to form homogeneous solutions with further stirring for 30 min. Each solution of both with and without Ce^{3+} dopants was adjusted the level of acid or alkali until reaching at the pH of 10 using 3 M NaOH, poured into each of stainless steel autoclave with a Teflon liner, and heated at 180°C for 20 h. At the conclusion of the process, the autoclaves were cooled to room temperature. The products were separated centrifugally, washed with deionized water and absolute ethanol several times, and dried at 80°C for 12 h.

The phase of the samples was characterized by X-ray diffraction (XRD) using a Philips X'Pert MPD X-ray diffractometer with CuK_α irradiation at λ = 1.5406 Å. The surface morphology was investigated by field emission scanning electron microscope (FE-SEM, JEOL JSM 6335F) and transmission electron microscope (TEM, JEOL, JEM2100) operated at the accelerating voltage of 35 and 200 kV, respectively. Raman and FTIR spectra were recorded on HORIBA JOBIN YVON T64000 Raman spectrometer with 50 mW and 514.5 nm wavelength Ar green laser and BRUKER TENSOR27 Fourier transform inferred (FTIR) spectrometer with KBr as a diluting agent and operated in the ranges of 100–1,000 cm^{-1} and 400–4,000 cm^{-1}, respectively. X-ray photoelectron spectroscopy (XPS) of the products was carried out via an Axis Ultra DLD, Kratos Analytical Ltd., with a monochromated Al K_α (1486.6 eV) radiation as the excitation source at 15 kV. All obtained spectra were calibrated to a C1s electron peak at 285.1 eV. UV-visible absorption spectra of an ethanol suspension of 0–3% Ce doped Bi_2MoO_6 samples were recorded under a Lambda 25, Perkin Elmer UV-visible spectrophotometer.

3. Results and Discussion

The typical XRD patterns as shown in Figure 1 reveal the phase and purity of the as-obtained 0–3% Ce doped Bi_2MoO_6 samples. All peaks of the undoped and Ce doped Bi_2MoO_6 samples were specified as the single phase orthorhombic Bi_2MoO_6 structure (JCPDS card number 73-2020 [11]). The presence of sharp and intense peaks confirmed the formation of highly crystalline nanomaterials. Furthermore, the absence of any impurity related peaks indicates that Ce^{3+} ions were successfully doped into Bi_2MoO_6 nanostructure. However, the intensity ratio of the (060) peak to the (131) peak of 3% Ce doped Bi_2MoO_6 sample is 1.66, obviously larger than the undoped Bi_2MoO_6 which is equivalent to 0.60 [12]. This important result indicates that the crystal has special anisotropic growth along the [0b0] direction.

The morphology and particle sizes of the Ce doped Bi_2MoO_6 with different contents of Ce ions were investigated by SEM as shown in Figure 2. It can be seen that the samples were comprised of a large number of nanoplates with diameters ranging between 0.1 and 0.3 μm and <100 nm thick. The surfaces of these nanoplates are smooth. Interestingly, when the samples were doped by different Ce concentrations, Ce doped Bi_2MoO_6 are still to be nanoplates. These show that Ce doping concentration had little effect on the shape of the products. Clearly, morphology and particle sizes of

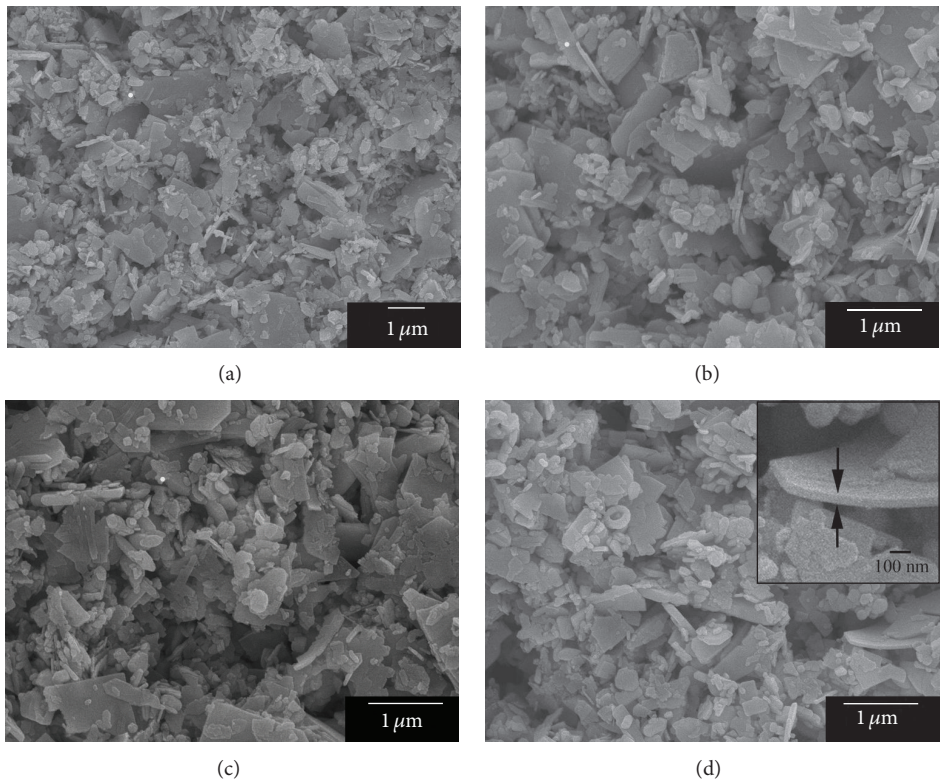

Figure 2: SEM images of the nanostructured ZnO of (a) undoped Bi_2MoO_6, (b) 1% Ce doped Bi_2MoO_6, and ((c), (d)) 3% Ce doped Bi_2MoO_6.

the Ce doped Bi_2MoO_6 nanoplates were consistent with pure Bi_2WO_6.

More information of the structure was obtained by TEM observation as shown in Figure 3. It confirms that the undoped Bi_2MoO_6 nanoplates have an average diameter of about 0.2 μm, in accordance with the SEM analysis. Obviously, some of lighter color parts can be seen, due to the difference in the contrast in TEM, mainly related to the difference in thickness of the samples. Furthermore, the 3% Ce doped Bi_2MoO_6 sample was composed of square nanoplates with ~100 nm thick edge. The selected area electron diffraction (SAED) patterns clearly demonstrate the single crystalline nature of the nanoplates. Interestingly, the SAED patterns taken on the whole single nanoplate show single crystalline patterns with sharp diffraction bright spots, giving the [100] zone axis character of orthorhombic Bi_2MoO_6. Based on the above XRD results, it is reasonable to conclude that the nanoplates preferentially grew along the [010] direction.

The chemical composition of 3% Ce doped Bi_2MoO_6 nanoplates was investigated by XPS spectroscopy as shown in Figure 4 and was calibrated using C1s peak at 285.1 eV. The Bi4f peaks of the 3% Ce doped Bi_2MoO_6 nanoplates appear at 159.52 eV of $4f_{7/2}$ and 164.80 eV of $4f_{5/2}$, corresponding to Bi^{3+} [4, 13–15]. Additional weak spin-orbit doublet peaks with binding energy of 157.92 eV for Bi $4f_{7/2}$ and 163.40 eV for Bi $4f_{5/2}$ are also detected, suggesting that some of bismuth exist as the $(+3-x)$ valence state [16]. Probably, the $Bi^{(+3-x)}$ formal oxidation state could be attributed to the substoichiometric phase within the microsized plates [16]. The production of lower oxidation state results in the presence of oxygen vacancies inside. The Mo3d spectrum showed spin-orbit splitting of the Mo3d levels at 232.84 eV and 236.00 eV, corresponding to the $3d_{5/2}$ and $3d_{3/2}$ orbitals [4, 13, 17, 18]. The spin-orbit splitting between $Mo3d_{5/2}$ and $Mo3d_{3/2}$ signals of Ce doped Bi_2MoO_6 nanoplates was set to 3.16 eV which are consistent with the previous reports [17]. However, single spin-orbit doublets showed peaks with binding energies of 231.3 eV ($Mo3d_{5/2}$) and 234.6 eV ($Mo3d_{3/2}$). These peaks are associated with Mo in formal (+6) oxidation state [19, 20]. The O_{1s} binding energy of 530.60 eV was in agreement with the literature value [4]. The O element might come from two kinds of chemical states: crystal lattice oxygen and adsorbed oxygen. The triple peaks of O_{1s} core at 529.30 eV, 530.45 eV, and 531.32 eV are attributed to the presence of Bi–O, Mo–O and Ce–O bonds in 3% Ce doped Bi_2MoO_6 sample [13]. The O_{1s} binding energy of 532.58 eV is due to the adsorbed oxygen. The XPS Ce3d peaks of cerium compounds are well known to be complicated because of hybridization of the Ce4f orbital with ligand orbital and fractional occupancy of the valence 4f orbital. The XPS spectrum of the $3d_{5/2}$ cerium level is therefore composed of three structures in the case of CeO_2 and only two structures in the case of Ce_2O_3 or other Ce^{3+} compounds [21]. The peaks at 880.73 eV, 884.34 eV, and 887.57 eV are due to $3d_{5/2}$ spin-orbit states, and those peaks at 898.68 eV, 901.94 eV, and 905.11 eV are due to the corresponding $3d_{3/2}$ states. The spin-orbit splitting is about 17.6 eV. The highest binding energy peaks located at about 902 eV and 884 eV are the result of a $Ce3d^9 4f^1 O2p^6$ of Ce(III)

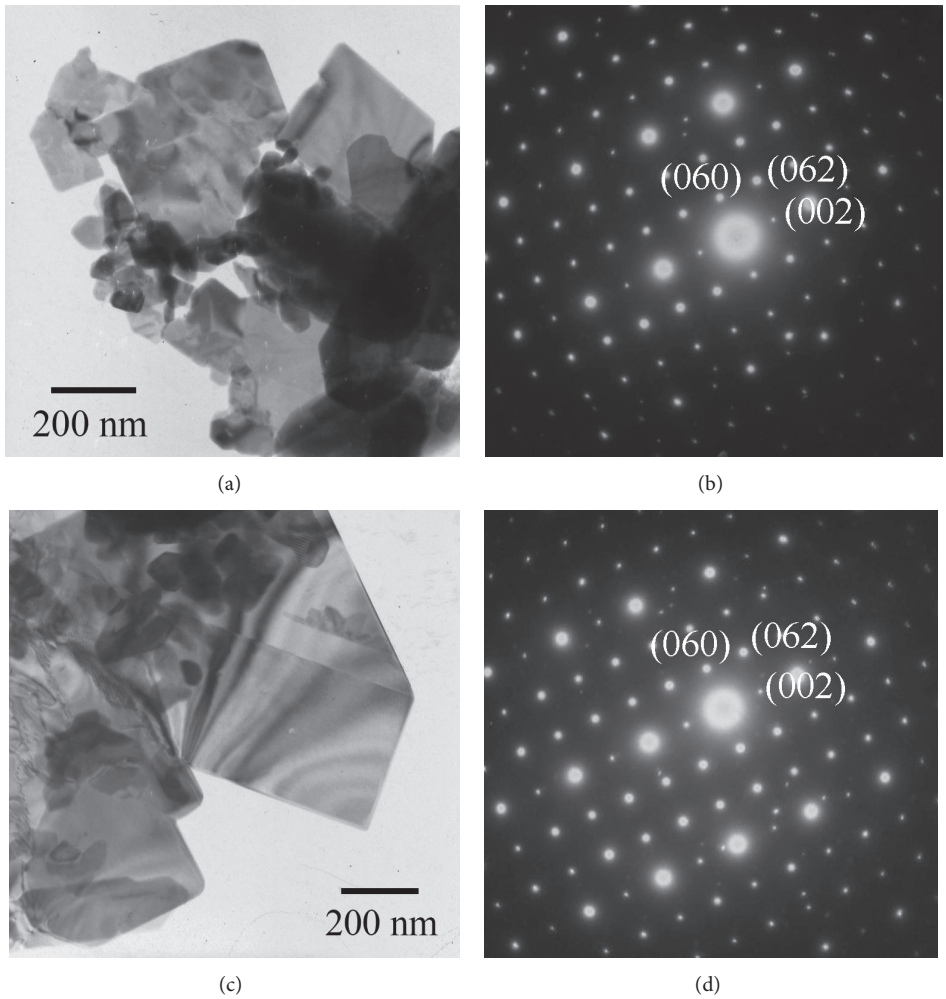

Figure 3: TEM images and SAED patterns of ((a), (b)) undoped Bi_2MoO_6, and ((c), (d)) 3% Ce doped Bi_2MoO_6.

in Ce_2O_3 in final state. The lowest binding energies located at 898.68 eV and 880.74 eV are the result of $Ce3d^9 4f^2$ $O2p^4$ [10, 21, 22]. The peaks at 887.57 eV and 905.11 eV are shakedown features resulting from the transfer of one or two electrons from a filled O2p orbital to an empty Ce4f orbital, that is, $Ce3d^9 4f^2$ $O2p^4$ and $Ce3d^9 4f^1$ $O2p^5$ Ce(IV) in the final states. Therefore, from the above results it is quite clear that there is coexistence of Ce^{3+} and Ce^{4+} in this sample [10, 21].

Bi_2MoO_6 crystal is built up of perovskite-like $(MoO_4)^{2-}$ and fluorite-like $(Bi_2O_2)^{2+}$ layers. Its room temperature and ambient pressure structure is orthorhombic (space group symmetry $P2_1ab$). A standard group theoretical analysis for the $P2_1ab$ room temperature phase of Bi_2MoO_6 unit cell leads to 108 degrees of freedom at the Brillouin zone center (Γ point). The optical modes are distributed among the irreducible representation of the factor group C_{2v} as $26A_1 + 27A_2 + 26B_1 + 26B_2$. Selection rules state that the A_1, B_1, and B_2 are both Raman and IR active whereas the A_2 modes are only Raman active [23–25].

Raman spectra of 0–3% Ce doped Bi_2MoO_6 samples are shown in Figure 5. It is well known that the bands in the 180–500 cm^{-1} range originated from the bending, wagging, and external modes by directly correlating the Mo–O bonds, and the 700–900 cm^{-1} region originated from the stretching vibration modes of the MoO_6 octahedrons. Raman peaks at 323, 345, and 400 cm^{-1} corresponded to the E_u symmetry bending modes. Raman modes near 293 cm^{-1} seemed to be from the E_g bending vibration. The band at 144 cm^{-1} was assigned as the lattice modes of Bi^{3+} atoms mainly in the direction normal to the layers. The strong band at 792 cm^{-1} was assigned to A_{1g} mode of Mo–O stretching vibration of the distorted MoO_6 octahedrons. The shoulder peak at 715 cm^{-1} was identified to the E_u asymmetric stretching of MoO_6 octahedrons involving the vibration of the equatorial oxygen atoms within the layers. The band at 841 cm^{-1} was assigned as the A_{2u} symmetric and asymmetric stretching vibrations of the MoO_6 octahedrons, relating to the motion of the apical oxygen atoms normal to the layers. When the Ce was doped into the samples, the strong bands at 792 cm^{-1} and two shoulder peaks at 715 and 840 cm^{-1} also slightly shifted to 713, 791, and 838 cm^{-1}, confirming an effective substitution

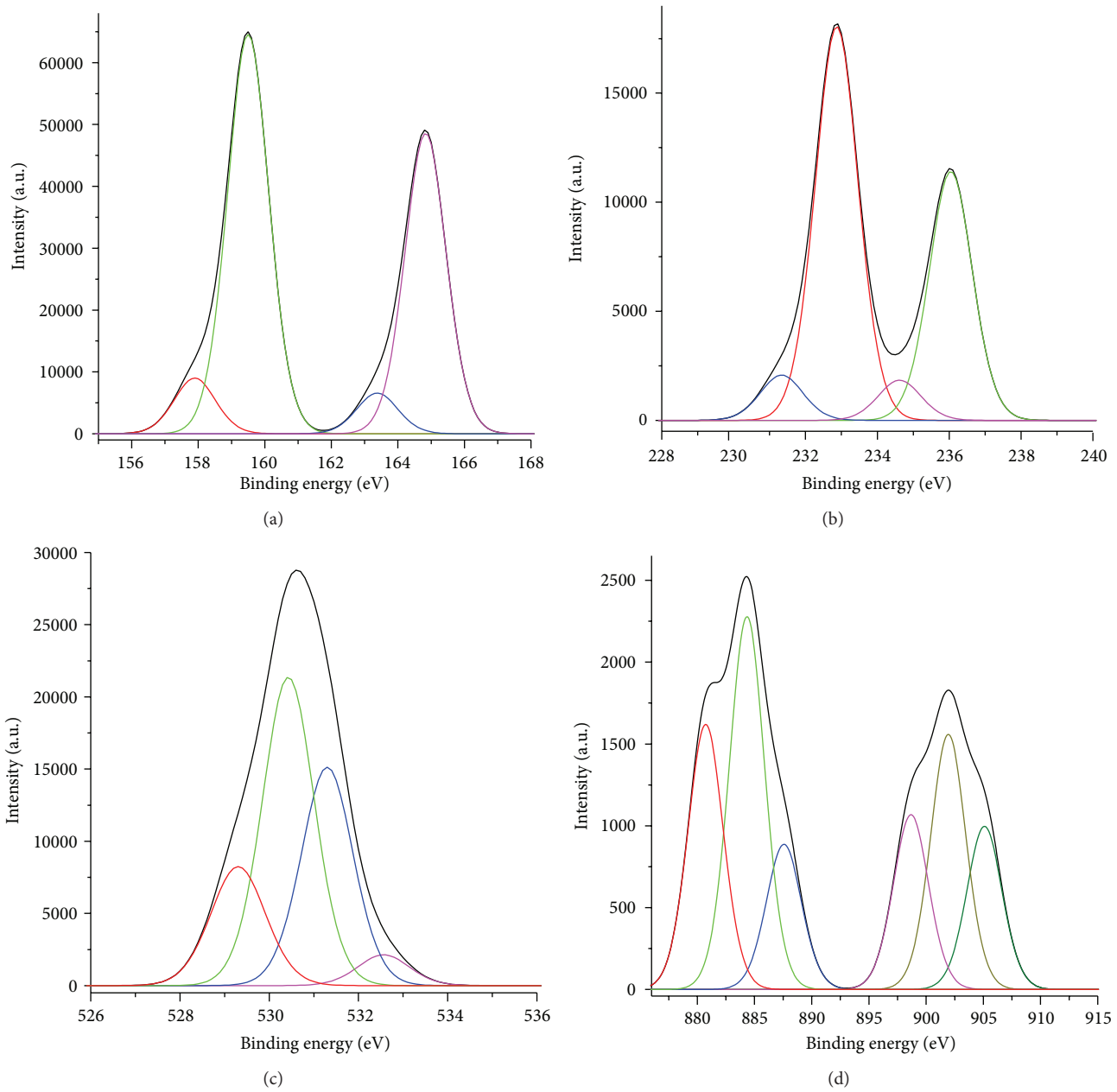

FIGURE 4: XPS spectra of the 3% Ce doped Bi_2MoO_6 nanoplates for (a) Bi4f, (b) Mo3d, (c) O_{1s}, and (d) Ce4f.

of Bi^{3+} ions by Ce^{3+} ions in the as-prepared nanocrystals, as also revealed by the XRD analysis [23–26].

FTIR spectra of the samples (Figure 6) show the band in the 400–900 cm^{-1} range, corresponding to Bi–O stretching and bending, Mo–O stretching, and Mo–O–Mo bridging stretching modes of Bi_2MoO_6. The bands at 843 and 797 cm^{-1} were assigned as the asymmetric and symmetric stretching modes of MoO_6 relating to vibrations of apical oxygen atoms, respectively. The 731 cm^{-1} mode was attributed to the asymmetric stretching vibration of the equatorial oxygen atoms of MoO_6 octahedrons. Those at 603 and 570 cm^{-1} were specified as the bending vibrations of MoO_6. Weak bands at 409 and 448 cm^{-1} were attributed to the stretching and bending vibrations of BiO_6 octahedrons [2, 26].

The UV-visible absorption spectra of the undoped and Ce doped Bi_2MoO_6 are shown in Figure 7. They show the strong absorption in the UV and visible-light regions. It should be noted that the maximum absorption was detected at 321 nm for 3% Ce doped Bi_2MoO_6, obviously blue shifted compared to that of Bi_2MoO_6 at 383 nm. For a crystalline semiconductor, the optical absorption near the band edge follows the equation $\alpha h\nu = A(h\nu - E_g)^{n/2}$, where α, ν, E_g, and A are the absorption coefficient, photonic frequency, energy gap, and a constant, respectively [2, 3]. For Bi_2MoO_6, the value of n is 1 for the direct transition. The plot of $(\alpha h\nu)^2$ versus photon energy ($h\nu$) of undoped and Ce doped Bi_2WO_6 was estimated from the intercepts of the tangents to the plots which are 1.86 eV for pure Bi_2MoO_6 and 2.04 eV for 3%

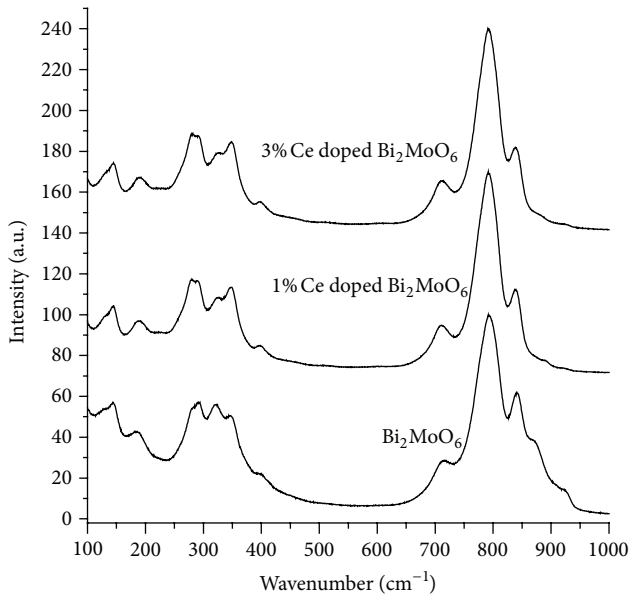

Figure 5: Raman spectra of undoped, 1% Ce doped, and 3% Ce doped Bi_2MoO_6 samples.

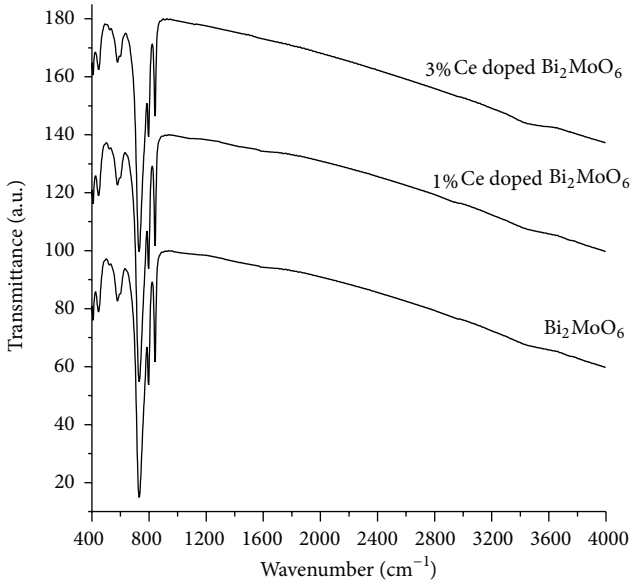

Figure 6: FTIR spectra of undoped, 1% Ce doped, and 3% Ce doped Bi_2MoO_6 samples.

Ce doped Bi_2MoO_6 which imply the possible application for visible-light photocatalysis.

4. Conclusions

0–3% Ce doped orthorhombic Bi_2MoO_6 nanoplates were successfully synthesized by the hydrothermal method. The experimental results presented that the as-synthesized products were orthorhombic Bi_2MoO_6 with the growth along the [010] direction. UV-visible absorption spectra show strong absorption due to the intrinsic energy gap transition of Bi_2MoO_6.

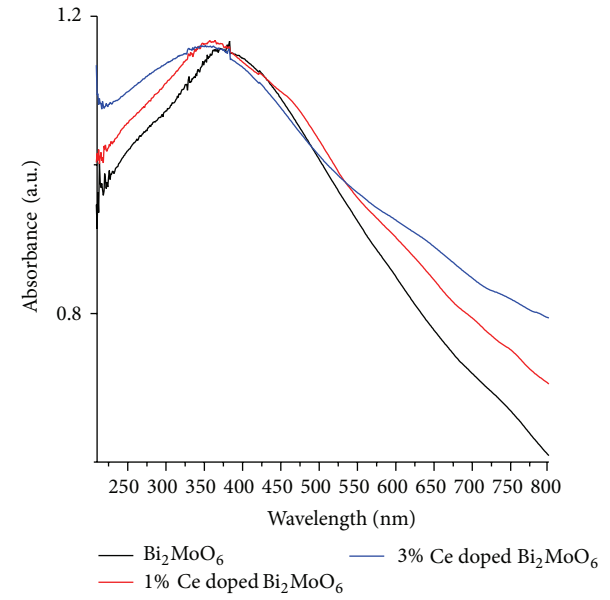

(a)

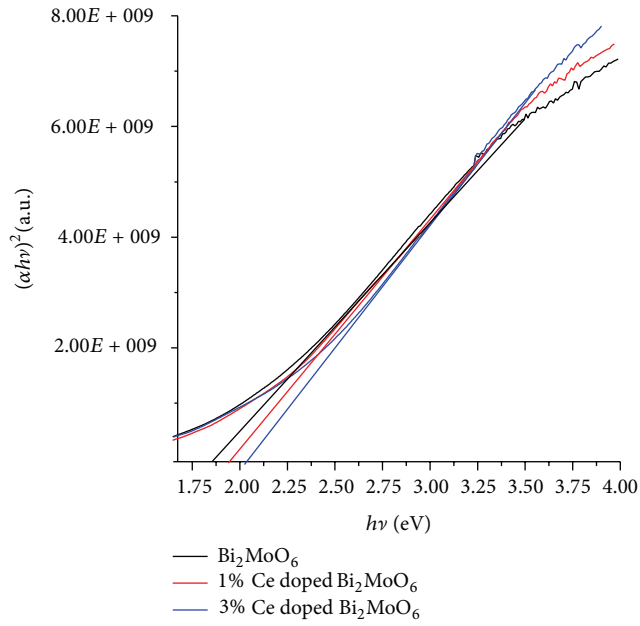

(b)

Figure 7: (a) UV-visible absorption and (b) $(\alpha h\nu)^2$ versus $h\nu$ curves of undoped, 1% Ce doped, and 3% Ce doped Bi_2MoO_6 samples.

Conflict of Interests

The authors declare that there is no conflict of interests regarding the publication of this paper.

Acknowledgment

The authors are extremely grateful to the Prince of Songkla University, Hat Yai, Songkhla, Thailand, for providing financial support through contract no. SCI560002S.

References

[1] Y. Shi, S. Feng, and C. Cao, "Hydrothermal synthesis and characterization of Bi_2MoO_6 and Bi_2WO_6," *Materials Letters*, vol. 44, no. 3, pp. 215–218, 2000.

[2] M. Zhang, C. Shao, P. Zhang et al., "Bi_2MoO_6 microtubes: controlled fabrication by using electrospun polyacrylonitrile microfibers as template and their enhanced visible light photocatalytic activity," *Journal of Hazardous Materials*, vol. 225-226, pp. 155–163, 2012.

[3] C. Xu, D. Zou, L. Wang, H. Luo, and T. Ying, "γ-Bi_2MoO_6 nanoplates: surfactant-assisted hydrothermal synthesis and optical properties," *Ceramics International*, vol. 35, no. 5, pp. 2099–2102, 2009.

[4] Y. Miao, G. Pan, Y. Huo, and H. Li, "Aerosol-spraying preparation of Bi_2MoO_6: a visible photocatalyst in hollow microspheres with a porous outer shell and enhanced activity," *Dyes Pigments*, vol. 99, pp. 382–389, 2013.

[5] X. Wang, F. Gu, L. Li, G. Fang, and X. Wang, "A facile mixed-solvothermal route to γ-Bi_2MoO_6 nanoflakes and their visible-light-responsive photocatalytic activity," *Materials Research Bulletin*, vol. 48, pp. 3761–3765, 2013.

[6] A. Martínez-de la Cruz and S. Obregón Alfaro, "Synthesis and characterization of γ-Bi_2MoO_6 prepared by co-precipitation: photoassisted degradation of organic dyes under vis-irradiation," *Journal of Molecular Catalysis A: Chemical*, vol. 320, no. 1-2, pp. 85–91, 2010.

[7] E. L. Cuéllar, A. Martínez-De La Cruz, K. H. L. Rodríguez, and U. O. Méndez, "Preparation of γ-Bi_2MoO_6 thin films by thermal evaporation deposition and characterization for photocatalytic applications," *Catalysis Today*, vol. 166, no. 1, pp. 140–145, 2011.

[8] W. Yin, W. Wang, and S. Sun, "Photocatalytic degradation of phenol over cage-like Bi_2MoO_6 hollow spheres under visible-light irradiation," *Catalysis Communications*, vol. 11, no. 7, pp. 647–650, 2010.

[9] J. Xie, D. Jiang, M. Chen et al., "Preparation and characterization of monodisperse Ce-doped TiO_2 microspheres with visible light photocatalytic activity," *Colloids and Surfaces A: Physicochemical and Engineering Aspects*, vol. 372, no. 1–3, pp. 107–114, 2010.

[10] M. Nasir, S. Bagwasi, Y. Jiao, F. Chen, B. Tian, and J. Zhang, "Characterization and activity of the Ce and N co-doped TiO_2 prepared through hydrothermal method," *Chemical Engineering Journal*, vol. 236, pp. 388–397, 2014.

[11] Powder Diffract. File, JCPDS Internat. Centre Diffract. Data, Pa, USA, 2001.

[12] Y. Zheng, F. Duan, J. Wu, L. Liu, M. Chen, and Y. Xie, "Enhanced photocatalytic activity of bismuth molybdates with the preferentially exposed 010 surface under visible light irradiation," *Journal of Molecular Catalysis A: Chemical*, vol. 303, no. 1-2, pp. 9–14, 2009.

[13] T. Zhou, J. Hu, and J. Li, "Er^{3+} doped bismuth molybdate nanosheets with exposed 010 facets and enhanced photocatalytic performance," *Applied Catalysis B: Environmental*, vol. 110, pp. 221–230, 2011.

[14] C. Wang, C. Shao, Y. Liu, and L. Zhang, "Photocatalytic properties BiOCl and Bi_2O_3 nanofibers prepared by electrospinning," *Scripta Materialia*, vol. 59, no. 3, pp. 332–335, 2008.

[15] B. Yuan, C. Wang, Y. Qi et al., "Decorating hierarchical Bi_2MoO_6 microspheres with uniformly dispersed ultrafine Ag nanoparticles by an in situ reduction process for enhanced visible light-induced photocatalysis," *Colloids and Surfaces A*, vol. 425, pp. 99–107, 2013.

[16] L. Wu, J. Bi, Z. Li, X. Wang, and X. Fu, "Rapid preparation of Bi_2WO_6 photocatalyst with nanosheet morphology via microwave-assisted solvothermal synthesis," *Catalysis Today*, vol. 131, pp. 15–20, 2008.

[17] Z. Li, L. Gao, and S. Zheng, "SEM, XPS, and FTIR studies of MoO_3 dispersion on mesoporous silicate MCM-41 by calcination," *Materials Letters*, vol. 57, no. 29, pp. 4605–4610, 2003.

[18] X. Zeng, X. Zhang, M. Yang, and Y. Qi, "A facile hydrothermal method for the fabrication of one-dimensional MoO_3 nanobelts," *Materials Letters*, vol. 112, pp. 87–89, 2013.

[19] B. M. Sánchez, T. Brousse, C. R. Castro, V. Nicolosi, and P. S. Grant, "An investigation of nanostructured thin film α-MoO_3 based supercapacitor electrodes in an aqueous electrolyte," *Electrochimica Acta*, vol. 91, pp. 253–260, 2013.

[20] M. Rouhani, Y. L. Foo, J. Hobley et al., "Photochromism of amorphous molybdenum oxide films with different initial Mo5+ relative concentrations," *Applied Surface Science*, vol. 273, pp. 150–158, 2013.

[21] H. Borchert, Y. V. Frolova, V. V. Kaidiev et al., "Electronic and chemical properties of nanostructured cerium dioxide doped with praseodymium," *Journal of Physical Chemistry B*, vol. 109, no. 12, pp. 5728–5738, 2005.

[22] M. Faisal, A. A. Ismail, A. A. Ibrahim, H. Bouzid, and S. A. Al-Sayari, "Highly efficient photocatalyst based on Ce doped ZnO nanorods: controllable synthesis and enhanced photocatalytic activity," *Chemical Engineering Journal*, vol. 229, pp. 225–233, 2013.

[23] M. MącZka, P. T. C. Freire, C. Luz-Lima, W. Paraguassu, J. Hanuza, and J. Mendes Filho, "Pressure-induced phase transitions in ferroelectric Bi_2MoO_6—a Raman scattering study," *Journal of Physics Condensed Matter*, vol. 22, no. 1, Article ID 015901, 2010.

[24] M. Mączka, W. Paraguassu, L. Macalik, P. T. C. Freire, J. Hanuza, and J. Mendes Filho, "A Raman scattering study of pressure-induced phase transitions in nanocrystalline Bi_2MoO_6," *Journal of Physics Condensed Matter*, vol. 23, no. 4, Article ID 045401, 2011.

[25] M. Mączka, L. Macalik, K. Hermanowicz, L. Kępiński, and J. Hanuza, "Synthesis and phonon properties of nanosized aurivillius phase of Bi_2MoO_6," *Journal of Raman Spectroscopy*, vol. 41, no. 10, pp. 1289–1296, 2010.

[26] L. Zhang, T. Xu, X. Zhao, and Y. Zhu, "Controllable synthesis of Bi_2MoO_6 and effect of morphology and variation in local structure on photocatalytic activities," *Applied Catalysis B: Environmental*, vol. 98, no. 3-4, pp. 138–146, 2010.